Inversion of vector-acoustic data in a local domain

Colton Kohnke & Paul Sava, Center for Wave Phenomena, Colorado School of Mines

SUMMARY

Advancements in marine seismic acquisition facilitate recording of vector-acoustic data, comprised of both the pressure and particle velocity wavefields. Having access to additional components of the seismic wavefield can aid efforts to image the subsurface. In order to utilize this extra information, we propose applying the adjoint state method to the vector-acoustic data to constrain the subsurface models. Gradient constructed by the adjoint state method are used to invert for the subsurface model parameters. The process of constructing gradients and inverting for the model parameters requires expensive wavefield computations. Much of these computations are wasted on wavefield propagation through regions of the model that do not change when the anomaly is localized to a small region of interest, such as in time-lapse applications. Since the anomaly is small and spatially constrained, we implement the method of multiple point sources to localize the gradient calculation and inversion to the region of interest. Localization of the wavefields constricts the simulation to the domain of interest, speeding up the calculation of the gradient and inversion.

INTRODUCTION

Marine seismic surveys typically use airguns that act as monopole sources, and record the pressure wavefield at streamer locations. However, recent advancements in marine seismic acquisition technology allow for recording of vector acoustic seismic data, comprised of both pressure and particle velocity wavefields (Robertsson et al., 2008). New marine seismic acquisition systems are capable of generating both monopole and dipole sources (Halliday et al., 2012). Having access to the full wavefield, i.e. both vector and scalar components, creates opportunities for a more accurate understanding the subsurface. Specifically, using all the components of the wavefield improves reverse-time migration (RTM) by reducing artifacts and improving illumination (Fleury and Vasconcelos, 2013; Ravasi et al., 2015), and full waveform inversion (FWI) by providing constraints on the subsurface parameters (Zhong and Liu, 2019).

This paper outlines how to utilize vector-acoustic data to build FWI gradients using the adjoint state method (Plessix, 2006). The method requires the state variable (the wavefield from the sources in forward time) and the adjoint variable (the wavefield from the receivers in reverse time). The gradient is the zero-lag cross-correlation between the state and adjoint variables. Once the model is updated in the direction of the gradient, the state and adjoint variables need to be recomputed in the updated model for the next model update.

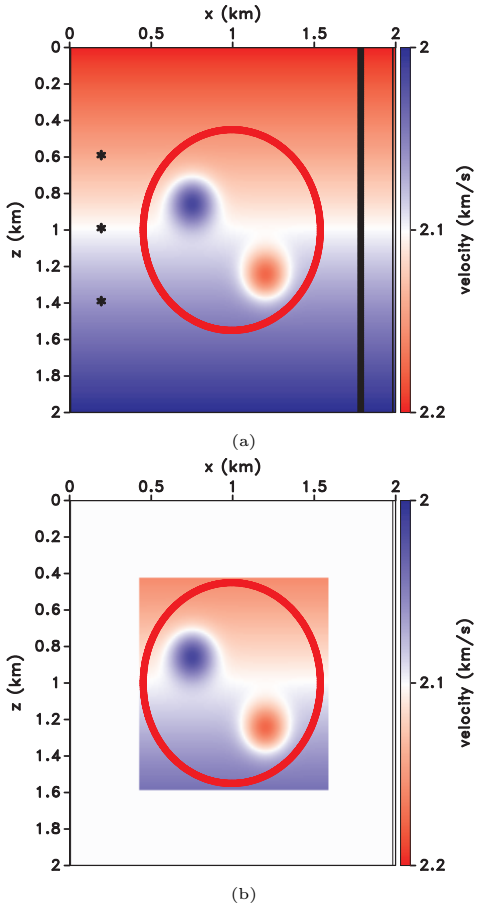

Figure 1: The a) full and b) local domains.

When the model is constrained to change in a small region of interest, such as in time-lapse seismic inversion or salt boundary delineation (Willemsen et al., 2016), much of the time computing the state and adjoint variables is wasted on propagating wavefields through unchanging regions of the model. Since the model is only updated within the small region of interest, we utilize the method of multiple point sources (MPS) as in van Manen et al. (2007), Vasmel and Robertsson (2016), and Kohnke and Sava (2018) to localize and reduce the cost of computing the wavefields. The MPS method takes the pressure and particle velocity measured in the full domain and creates synthetic sources on the boundary of a local domain of interest. These sources create wavefields inside the local domain as if they were propagating inside the full domain, and cancel out wavefields that leave the domain. If the model is updated within the local region, the wavefield that propagates inside the local domain matches the wavefield in the full domain, but

the sources no longer completely cancel out the outgoing wavefields. Once the sources on the local domain are calculated, the modeling for the state and adjoint variables for FWI can be carried out using the local domain, decreasing the computational cost. The cost decreases every time the state and adjoint variables are computed using the local domain, thus significantly reducing the inversion cost.

VECTOR-ACOUSTIC OPERATOR

The first-order vector-acoustic wave equation is

$$\rho \frac{\partial \mathbf{v}}{\partial t} + \nabla p = \mathbf{f} \tag{1}$$

$$\frac{1}{\rho c^2}\frac{\partial p}{\partial t} + \nabla \cdot \mathbf{v} = q. \tag{2}$$

These equations link particle velocity $\mathbf{v}(\mathbf{x}, t)$ with the pressure $p(\mathbf{x}, t)$ from dipole $\mathbf{f}(\mathbf{x}, t)$ and monopole $q(\mathbf{x}, t)$ sources. The wavefields propagate in a medium with spatially variable density $\rho(\mathbf{x})$ and velocity $c(\mathbf{x})$. Equations 1 and 2 can be written in a compact operator form as

$$\mathbf{L}\mathbf{u} = \mathbf{d}, \tag{3}$$

where

$$\mathbf{L} = \begin{bmatrix} \rho\dfrac{\partial}{\partial t} & \nabla \\ \nabla\cdot & \dfrac{1}{\rho c^2}\dfrac{\partial}{\partial t} \end{bmatrix} \tag{4}$$

$$\mathbf{u} = \begin{bmatrix} \mathbf{v} \\ p \end{bmatrix}, \tag{5}$$

$$\mathbf{d} = \begin{bmatrix} \mathbf{f} \\ q \end{bmatrix}. \tag{6}$$

We solve equation 3 iteratively using finite-differences, by alternating between particle velocity at the current time-step and pressure at the next time-step. The pressure and particle velocity grids are staggered in space and time on a Yee grid (Yee, 1966). The wavefield term $\mathbf{u}$ is the state variable used for building FWI gradients.

The adjoint operator is written as

$$\mathbf{L}^\dagger \mathbf{a} = \mathbf{g}, \tag{7}$$

where

$$\mathbf{L}^\dagger = \begin{bmatrix} \rho\left(\dfrac{\partial}{\partial t}\right)^\dagger & -\nabla \\ -\nabla\cdot & \dfrac{1}{\rho c^2}\left(\dfrac{\partial}{\partial t}\right)^\dagger \end{bmatrix}, \tag{8}$$

and $\mathbf{g}(\mathbf{x}, t)$ is the adjoint source, often the data difference at the receivers in FWI applications, and $\mathbf{a}(\mathbf{x}, t)$ defined by

$$\mathbf{a} = \begin{bmatrix} \mathbf{f} \\ q \end{bmatrix} \tag{9}$$

is the adjoint variable. The adjoint operator is solved iteratively in reverse time, by alternating between the monopole term (q) at the last time-step and the dipole term ($\mathbf{f}$) at the previous time-step.

VECTOR-ACOUSTIC GRADIENTS

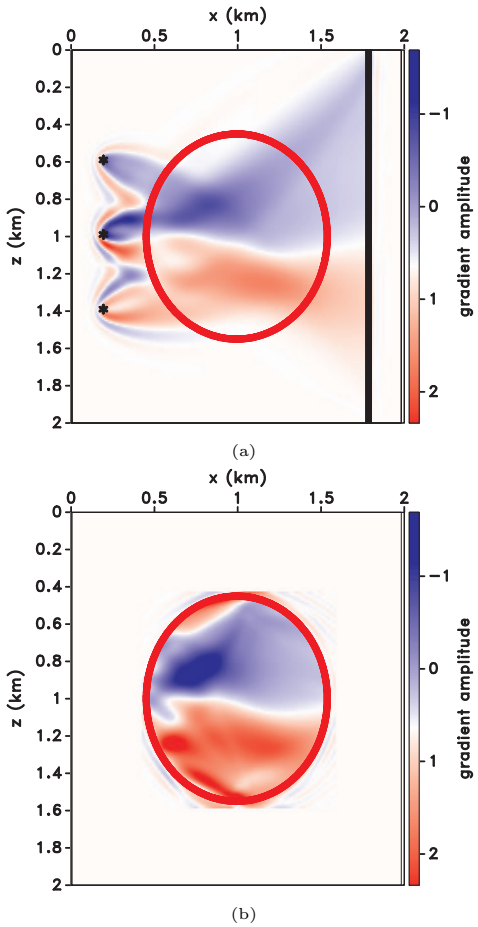

Figure 2: Gradients for the velocity update in the full (a) and local (b) domains. The density model is constant.

The objective function gradient is obtained by minimizing the augmented functional (Duan and Sava, 2016)

$$\mathcal{H} = \mathcal{J} - \mathcal{F}^\dagger \mathbf{a}. \tag{10}$$

Here, $\mathcal{J}$ the objective function we are minimizing, $\mathbf{a}(\mathbf{x}, t)$ is the adjoint variable and $\mathcal{F}$ is the physical constraint indicating that the state variable $\mathbf{u}(\mathbf{x}, t)$ is the result of a linear process described by wave equation represented by operator $\mathbf{L}$:

$$\mathcal{F} = \mathbf{L}\mathbf{u} - \mathbf{d} = 0. \tag{11}$$

Using the augmented functional and physical constraints we can derive two gradients: one to update velocity while density is constant, and one to update both velocity and density.

Constant density

We consider the constant density version of equations 1 and 2, and write the model parameter for inversion as

the slowness squared

$$m(\mathbf{x}) = \frac{1}{c^2(\mathbf{x})}. \tag{12}$$

The constrained gradient of the augmented functional in equation 10 is then

$$\frac{\partial \mathcal{H}}{\partial m} = \frac{\partial \mathcal{J}}{\partial m} - \sum_e \left[\left(\frac{\partial \mathcal{F}}{\partial m} \right)^\dagger \right] [\mathbf{a}] \tag{13}$$

and implies summation over time. The derivative of $\mathcal{F}$ with respect to the model parameter can be written

$$\frac{\partial \mathcal{F}}{\partial m} = \frac{\partial}{\partial m}(\mathbf{L}\mathbf{u} - \mathbf{d}) = \begin{bmatrix} 0 & 0 \\ 0 & \dfrac{\partial}{\partial t} \end{bmatrix} \begin{bmatrix} \mathbf{v} \\ p \end{bmatrix} = \frac{\partial p}{\partial t}. \tag{14}$$

The gradient is the zero time-lag cross-correlation of the state and adjoint variables:

$$\frac{\partial \mathcal{H}}{\partial m} = \frac{\partial \mathcal{J}}{\partial m} - \sum_e \sum_\tau \delta(\tau) \left(\dot{p} \star \mathbf{a}^q \right). \tag{15}$$

The dot over the pressure indicates the first time derivative. The superscript q of the adjoint variable denotes the scalar component corresponding to a monopole wavefield term.

The augmented functional $\mathcal{H}$ does not depend explicitly on the model parameter m, and therefore $\dfrac{\partial \mathcal{H}}{\partial m} = 0$, so we write the gradient of the objective function as

$$\frac{\partial \mathcal{J}}{\partial m} = \sum_e \sum_\tau \delta(\tau) \left(\dot{p}_s \star a_s^q \right). \tag{16}$$

The gradient in equation 16 can be used in inversion to update the model parameter m, after which a new gradient can be computed from the state and adjoint variables. This gradient term using the scalar component of the wavefield is the same as proposed by Akrami et al. (2017), but correctly accounts for the time derivative on the state variable pressure.

As an example, consider the velocity in Figure 1 to be the model used to compute the observed data at the receivers. The observed data for the local domain is a perfect redatum from the receivers to the surface of the local domain. The background model is the same, but without the Gaussian anomalies, and is used to compute the state and adjoint variables. The gradients for velocity created using equation 16 in the full and local domains are shown by Figure 2. While these gradients are scaled arbitrarily when used by the inversion algorithm, they are plotted on the same scale to show that they match in amplitude and general shape. The high intensity areas of the gradient correspond with the locations of the Gaussian anomalies in the true model. There are also high intensities near the local domain borders, which influence the inversion, but those can be compensated for by incorporating additional objective function terms (Li and Oldenburg, 1998), as opposed to only using a data objective function.

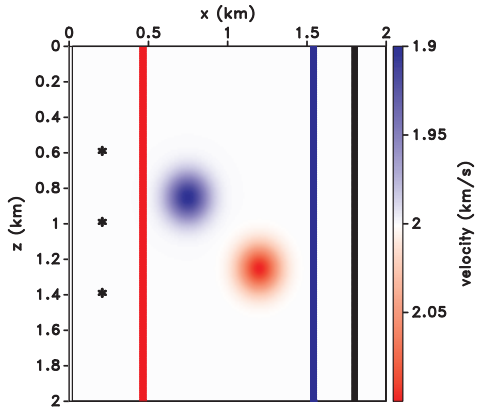

Figure 3: The true velocity model in the full domain. The local domain is the region between the red and blue vertical lines.

Variable density

Common practice for FWI is to use density as an unconstrained parameter to better match the data after updating the velocity model. This may yield geologically impossible density models which can be a hindrance if the FWI results are used for other applications, such as a starting model in gravity inversion. If we consider the density as an additional model parameter, we can constrain the density update in a way that makes geologic sense. For models defined with variable density, we define the model parameters by

$$m_1(\mathbf{x}) = \frac{1}{c(\mathbf{x})^2}, \tag{17}$$

$$m_2(\mathbf{x}) = \rho(\mathbf{x}). \tag{18}$$

Then, similarly to the preceding case, we write the derivative of $\mathcal{F}$ with respect to each model parameter as

$$\begin{aligned} \frac{\partial \mathcal{F}}{\partial m_1} &= \frac{\partial}{\partial m_1}(\mathbf{L}\mathbf{u} - \mathbf{d}) \\ &= \begin{bmatrix} 0 & 0 \\ 0 & \dfrac{1}{m_2}\dfrac{\partial}{\partial t} \end{bmatrix} \begin{bmatrix} \mathbf{v} \\ p \end{bmatrix} = \frac{1}{m_2}\frac{\partial p}{\partial t} \end{aligned} \tag{19}$$

$$\begin{aligned} \frac{\partial \mathcal{F}}{\partial m_2} &= \frac{\partial}{\partial m_2}(\mathbf{L}\mathbf{u} - \mathbf{d}) \\ &= \begin{bmatrix} \dfrac{\partial}{\partial t} & 0 \\ 0 & -\dfrac{m_1}{m_2^2}\dfrac{\partial}{\partial t} \end{bmatrix} \begin{bmatrix} \mathbf{v} \\ p \end{bmatrix} = \begin{bmatrix} \dfrac{\partial \mathbf{v}}{\partial t} \\ -\dfrac{m_1}{m_2^2}\dfrac{\partial p}{\partial t} \end{bmatrix}. \end{aligned} \tag{20}$$

We then find the gradients of the object function with respect to both model parameters as

$$\frac{\partial \mathcal{J}}{\partial m_1} = \frac{1}{m_2} \sum_e \sum_\tau \delta(\tau) \left(\dot{p} \star \mathbf{a}^q \right) \tag{21}$$

$$\frac{\partial \mathcal{J}}{\partial m_2} = \sum_e \sum_\tau \delta(\tau) \left(\sum_i \left(\dot{\mathbf{v}}^i \star \mathbf{a}^i \right) - \frac{m_1}{m_2^2} \left(\dot{p} \star \mathbf{a}^q \right) \right). \tag{22}$$

The derivative with respect to m_1 is a scaled version of what we found in equation 16. The derivative with respect to m_2 has components derived from both vector and scalar components of the state and adjoint variables. The summation over i is for all vector components of the state and adjoint fields. Equations 21 and 22 suggest that the particle velocity wavefield does not influence the velocity model, but all components of the wavefield contribute to the density model. Updating the model parameters is a two-step process. First, we use equation 21 to update the velocity model, then we use equation 22 to update the density model. Then we recompute the state and adjoint variables, as well as the gradient for the next iteration of the inversion.

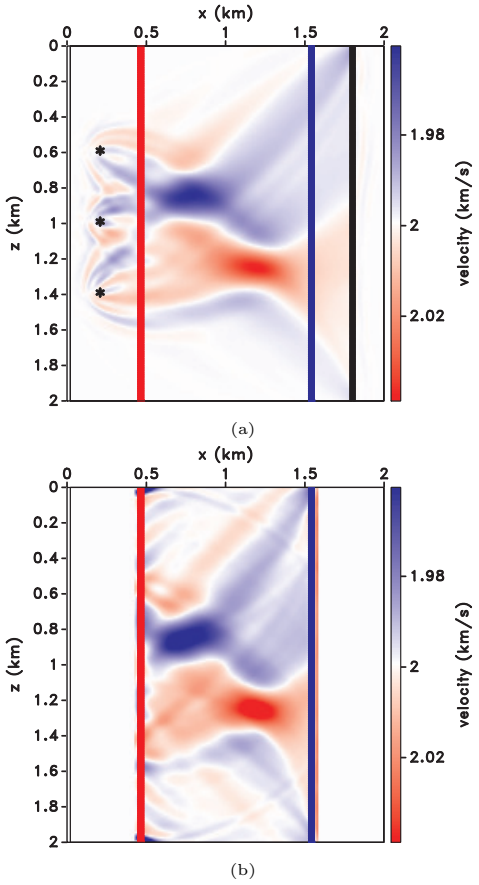

Figure 4: Final velocity model for the full (a) and local (b) domain inversions after 10 iterations of L-BFGS.

SYNTHETIC EXAMPLE

We consider a synthetic model with the true velocity model shown in Figure 3, and with initial model as a constant 2.0 km/s. The density model is also constant. The sources are on the left side of the model and the receivers are indicated by the vertical line on the right. The local domain is the region of the model between the red and blue vertical lines. The red line represents the surface to which sources are redatumed, from which we generate the state variable. The blue line is the surface to which the receivers are redatumed, from which we create the adjoint variable. In this case, we are assuming a perfect redatum onto the blue surface. In principle, redatuming can be achieved through an iterative least-squares problem linking the wavefield on the local domain surface (i.e. the model) to the observations at the receivers (i.e. the data).

We invert for the velocity model that minimizes the data difference on the local domain using a limited memory BFGS algorithm (Nocedal and Wright, 2006). After 10 iterations we obtain the models shown in Figure 4. The high intensity regions of the full domain model correspond with the positive and negative Gaussian anomalies. The local domain inversion also reconstructs the Gaussian anomalies, but includes some artifacts that streak throughout the model. These artifacts could be mitigated by incorporating additional constraints into the model objective functions, such as model smoothness constraints.

CONCLUSION

In applications where the model only changes in a local region of interest, it is much more cost efficient to use a local domain for wavefield simulations instead of the full domain. The forward and adjoint wavefields inside the local domain mimic the behavior of the wavefields in the full domain by using the method of multiple point sources, even after model alterations. The local FWI gradient can be constructed using these local wavefields, and be used to update the model. By using the vector-acoustic wave equations and the adjoint-state method, we can construct FWI gradients for the velocity and density models, updating both to minimize the data objective function.

The cost reduction allowed by using the local domain depends on its relative size to the full domain. The main speedup is due to shrinking the number of operations needed by spatial derivatives. A secondary speedup occurs by reducing the modeling time, as we do not need to simulate wavefields before the source reaches the local domain or after the wavefields leave the domain. These benefits occur at every iteration of the inversion, allowing for more complex inversions in less time than in the full domain.

ACKNOWLEDGMENTS

We thank the sponsors of the Center for Wave Phenomena, whose support made this research possible. The synthetic examples in this paper use the Madagascar open-source software package Fomel et al. (2013) freely available from `http://www.ahay.org`. We thank Theo Becker (ETH Zurich) for useful discussion.

REFERENCES

Akrami, S. M., P. Zheglova, and A. Malcolm, 2017, An algorithm for vector data full-waveform inversion: SEG Technical Program Expanded Abstracts 2017, Society of Exploration Geophysicists, 1568–1572.

Duan, Y., and P. Sava, 2016, Elastic wavefield tomography with physical model constraints: Geophysics, **81**, R447–R456.

Fleury, C., and I. Vasconcelos, 2013, Adjoint-state reverse time migration of 4C data: Finite-frequency map migration for marine seismic imaging: Geophysics, **78**, WA159–WA172.

Fomel, S., P. Sava, I. Vlad, Y. Liu, and V. Bashkardin, 2013, Madagascar: open-source software project for multi-dimensional data analysis and reproducible computational experiments: Journal of Open Research Software, **1**, e8.

Halliday, D., J. O. A. Robertsson, I. Vasconcelos, D.-J. van Manen, R. Laws, K. Özdemir, and H. Grønaas, 2012, Full-wavefield, towed-marine seismic acquisition and applications: SEG Technical Program Expanded Abstracts 2012, Society of Exploration Geophysicists, 1–5.

Kohnke, C., and P. Sava, 2018, Localized FWI for time-lapse monitoring: SEG Technical Program Expanded Abstracts 2018, 1389–1393.

Li, Y., and D. W. Oldenburg, 1998, 3-D inversion of gravity data: Geophysics, **63**, 109–119.

Nocedal, J., and S. Wright, 2006, Numerical optimization, *in* Springer.

Plessix, R.-E., 2006, A review of the adjoint-state method for computing the gradient of a functional with geophysical applications: Geophysical Journal International, **167**, 495–503.

Ravasi, M., I. Vasconcelos, A. Curtis, and A. Kritski, 2015, Vector-acoustic reverse time migration of Volve ocean-bottom cable data set without up/down decomposed wavefields: Geophysics, **80**, S137–S150.

Robertsson, J. O., I. Moore, M. Vassallo, K. Özdemir, D.-J. van Manen, and A. Özbek, 2008, On the use of multicomponent streamer recordings for reconstruction of pressure wavefields in the crossline direction: Geophysics, **73**, A45–A49.

van Manen, D.-J., J. O. A. Robertsson, and A. Curtis, 2007, Exact wave field simulation for finite-volume scattering problems: The Journal of the Acoustical Society of America, **122**, EL115—-EL121.

Vasmel, M., and J. O. A. Robertsson, 2016, Exact wavefield reconstruction on finite-difference grids with minimal memory requirements: Geophysics, **81**, T303–T309.

Willemsen, B., A. Malcolm, and W. Lewis, 2016, A numerically exact local solver applied to salt boundary inversion in seismic full-waveform inversion: Geophysical Journal International, **204**, 1703–1720.

Yee, K. S., 1966, Numerical solution of initial boundary value problems involving Maxwell's equations in isotropic media: IEEE Transactions on Antennas and Propagation, **14**, 302–307.

Zhong, Y., and Y. Liu, 2019, Source-independent time-domain vector-acoustic FWI: Geophysics, 1–50.